

## Supporting Information for

Potentially Important Contribution of Gas-Phase Oxidation of Naphthalene and Methyl-naphthalene to Secondary Organic Aerosol during Haze Events in Beijing

Guancong Huang<sup>1</sup>, Ying Liu<sup>1\*</sup>, Min Shao<sup>1,2</sup>, Yue Li<sup>1</sup>, Qi Chen<sup>1</sup>, Yan Zheng<sup>1</sup>, Zhijun Wu<sup>1</sup>, Yuechen Liu<sup>1</sup>, Yusheng Wu<sup>1†</sup>, Min Hu<sup>1</sup>, Xin Li<sup>1</sup>, Sihua Lu<sup>1</sup>, Chenjing Wang<sup>1</sup>, Junyi Liu<sup>1</sup>, Mei Zheng<sup>1</sup>, Tong Zhu<sup>1\*</sup>

<sup>1</sup> SKL-ESPC and BIC-ESAT, College of Environmental Sciences and Engineering, Peking University, Beijing 100871, China

<sup>2</sup> Institute for Environmental and Climate Research, Jinan University, Guangzhou 511443, China

<sup>†</sup> Now at Department of Physics, University of Helsinki, 00014 Helsinki, Finland.

### **This file includes:**

Supporting text

Supporting Table S1-S10

Supporting Figure S1-S16

Supporting references

Number of pages: 57

## 1. Data processing.

All the fitted signals by PTR-QiTOF were normalized using the sum of reagent ions ( $\text{H}_3\text{O}^+$  and  $\text{H}_2\text{O}(\text{H}_3\text{O})^+$ ) at the level of  $1 \times 10^6$  cps according to the following equation<sup>1</sup> (Eq S1):

$$\text{normalized ion signal} = \frac{i(\text{RH}^+)}{i(\text{H}_3[^{18}\text{O}]^+) \times 500 + X_r \times \frac{1}{T_r} \times 250 \times i(\text{H}_2\text{O})\text{H}_3[^{18}\text{O}]^+} \times 10^6 \quad (\text{Eq S1})$$

Where  $i(\text{RH}^+)$  represents the signals of protonated VOC ions,  $i(\text{H}_3[^{18}\text{O}]^+)$  and  $i((\text{H}_2\text{O})\text{H}_3[^{18}\text{O}]^+)$  are the isotopic ion signals for reagent ions ( $\text{H}_3\text{O}^+$  and  $(\text{H}_2\text{O})\text{H}_3\text{O}^+$ ). The relative abundance is 500 for  $i(\text{H}_3[^{18}\text{O}]^+)$  to  $i(\text{H}_3[\text{O}]^+)$ , and 250 for  $i((\text{H}_2\text{O})\text{H}_3[^{18}\text{O}]^+)$  to  $i((\text{H}_2\text{O})\text{H}_3\text{O}^+)$ .  $X_r$  is the factor reflecting the difference in rate constant for  $\text{R} + \text{H}_3\text{O}^+$  and  $\text{R} + (\text{H}_2\text{O})\text{H}_3\text{O}^+$  reactions.  $T_r$  is the relative transmission efficiency between  $(\text{H}_2\text{O})\text{H}_3[^{18}\text{O}]^+$  and  $\text{H}_3[^{18}\text{O}]^+$ .

The transmission efficiency for ions ( $T_r(\text{RH}^+)$ ) is proportional to  $\sqrt{m/Q(\text{RH}^+)}$  in TOF-MS system<sup>2</sup>. For species without authentic standard, their sensitivities were estimated based on the relationship between the relative transmission efficiency versus the square root of the ratios of  $m/Q$ . This method was very similar to that described by Taipale et al. (2008)<sup>3</sup>. In this study, the relative transmission curve was determined by calibration results from 40 VOC/IVOC gas standards, among which only those species with few fragment was used for transmission correction. The theoretical calibration factors were compared with measured values. It was found that the theoretical

calibration factors generally agreed well with the values determined from authentic standards (Figure S1). The measured sensitivities of acids and aldehydes were slightly higher than the theoretically predicted values by less than 10%. The theoretical sensitivities could be reliable within  $\pm 14\%$  for those compounds without standards.

## **2. Uncertainties for the gas phase oxidation product measurement.**

### **2.1 Measurement precision and detection limit for PTR-QiTOF**

Based on the calibration results, the measurement precision and detection limit for PTR-QiTOF were calculated. The precision of PTR-QiTOF measurement is determined by the counting statistics of the protonated ions, which is assumed to obey the Poisson distribution<sup>4</sup>. The mixing ratios for target compounds are calculated from the signals when the VOC catalyst is off by deducting the background signal with the catalyst on<sup>5</sup>. The measurement precision for toluene ( $m/z=93$ ), naphthalene ( $m/z=129$ ) and dichlorobenzene ( $m/z=147$ ) was 2.4%, 1.3% and 5.6%, respectively, when their mixing ratios are around 1 ppb. For most oxidation products, their mixing ratios are normally lower than 0.1 ppb in atmosphere. Here, the measurement precision was estimated to be within 15%.

The detection limits for PTR-QiTOF are defined as the mixing ratios that can be detected with a signal-to-noise ratio of 3. The background signal during the whole campaign was used to calculate detection limits, as listed in Table 1 and Table S1.

## 2.2 Effect of the Teflon tubing length to the loss of organic compounds.

Teflon tubing is widely used as the inlet between ambient air and the instrument because of its chemical inertness. The 8 meters long PFA Teflon tubing was necessary because the sampling port was away from the instrument. Before the campaign, several test experiments were conducted to examine the wall loss of VOCs/IVOCs upon the length of Teflon tubing including aldehyde, acid, aromatics and phenols. The saturation concentration ( $\log C^*$ ) of the authentic standards ranged from 5.7 to 9.5  $\mu\text{g}/\text{m}^3$ . The base case of wall loss test was conducted with gas standards through 2 m of Teflon tubing. The effect of tubing length was evaluated with the same 1/4 inch OD Teflon tubing by increasing the Teflon tubing length from 2 m to 10 m. The relative deviation of the concentration of the compounds could be calculated as:

$$\text{Relative deviation} = \frac{S_{L=x} - S_{L=2}}{S_{L=2}} \times 100\% \quad (\text{Eq S2})$$

Where  $x$  was the length of the Teflon tubing ( $x=2, 4, 6, 8, 10$  m);  $S_{L=x}$  was the measured mixing ratio of the gas standard after flowing through the  $x$  m-long Teflon tubing.

In these experiments, the gas standards were generated with certificated permeation tubes in the Dynacalibrator (VICI Metronics) or the cylinder gas. The constant gas standards with the mixing ratio of each compound about 1 ppb were introduced to the

Teflon tubing at a constant flowrate of 8 L/min. The flowrate during the tests was set as the same as that operated during the campaign.

Also, the effect of relative humidity (RH) was examined under dry, RH=25% and RH=50% conditions at room temperature (18 °C). It should be noticed that the actual water content was 3.84 g/m<sup>3</sup> (i.e. absolute humidity) under RH=25% at 18 °C, which was quite close to the value (3.89 g/m<sup>3</sup>) in the haze episodes when RH was 70% at ambient temperature of 2 °C. Thus, results from RH=25% conditions in laboratory could represent the most situations during the haze events.

The effect of inlet length and RH on the losses were presented in Figure S2. Generally, the relative deviations of concentrations for standards were found to be negative, less than 5% of compounds were lost on the Teflon wall and the losses were slightly increased with the length of tubing. RH didn't have a significant influence on the wall loss. In the case of RH=25% at 18 °C, the losses of standards were within 3–4%, which were in the range of the instrument precision. It indicates that the 8 m-long tubing used in the field campaign would be reasonable

For the I/SVOCs without authentic standards, the wall loss tests were conducted with the ambient air, assuming the mixing ratios of the target compounds were relatively stable in a short time. To minimize the possible interference, the tests were repeated eight times and the duration time of each test were shorten to within 15 min. Ambient

air samples were measured alternately through two sampling lines with the lengths of 8 m and 2 m, each measurement kept for ~7 min with the time resolution of 2 s. Variations of the average mixing ratios of the Nap oxidation products in the tests were presented in Figure S3. It was found that the average mixing ratios when the Teflon tubing was 2 m long was generally higher than that with 8 m-long Teflon tubing. The relative deviation was then calculated with Equation S2, and results were summarized in Table S2. The high volatility of phthalic anhydride ( $\log C^* = 4.3 \mu\text{g}/\text{m}^3$ ) lead to the less wall loss ( $-4.9 \pm 3.5\%$ ), which was consistent with the results for authentic standards with  $\log C^*$  ranging from 5.7 to 9.5  $\mu\text{g}/\text{m}^3$ . For the di-carbonyl compounds (i.e., 2-formylcinnamaldehyde ( $\log C^* = 2.2 \mu\text{g}/\text{m}^3$ ) and phthalaldehyde ( $\log C^* = 3.7 \mu\text{g}/\text{m}^3$ )), the wall losses were similar with the average value of  $-14.8 \pm 13.8\%$  and  $-13.7 \pm 7.9\%$  respectively. Phthalic acid, with the lowest volatility ( $\log C^* = -1.1 \mu\text{g}/\text{m}^3$ ), was observed to suffer the largest wall loss among the oxidation products ( $21.8 \pm 16.2\%$ ). As the relative deviations for 1,2-PhA fluctuated in a larger range (-1.7 to -41.5%) in the ambient tests, it would generate an additional error of  $\pm 28\%$  (wall loss uncertainty) in the quantification of 1,2-PhA.

### **2.3 Effect of the Teflon filter to the loss of organic compounds.**

The PTFE filter with 2.0  $\mu\text{m}$  pore size (Whatman Inc) used here is a popular sampling media for  $\text{PM}_{2.5}$  measurements, because it is very stable and inert to absorb gaseous compounds. During the campaign, the PTFE filter was usually replaced every day or

every 12 hours during haze episodes. Besides, a previous study showed that such PTFE filter is able to remove 99.7% of particles in ambient air<sup>6</sup>. The measurement accuracy of I/SVOCs would be affected by potential artifacts, includes: 1) positive artifact due to the penetration of tiny particles through the filter; 2) positive artifact caused by the re-evaporation from particle-phase SVOCs collected on the filter; 3) negative artifact attributed to the absorption of gas-phase SVOCs onto the filter or to the existing particles collected on the filter.

To determine the possible artifacts, test experiments on filter were performed before the campaign. Ambient air was sampled into the instrument without filter, with clean filter, and with dirty filter at a flowrate of 8 L/min, respectively. In the case of without filter, both gases and particles were sampled. It is mentioned the PM concentration was quite low during this test experiment. Thus, this scenario could be regarded as the total gaseous concentrations of target compounds. In the case of clean filter, the possible absorption of target compounds by the filter itself was examined. Later, the clean filter was replaced by a dirty filter, which has sampled particles for 24 hours beforehand. The dirty filter represented the condition that the filter had a high particle loading during haze events. As shown in Figure S4, it is found that the clean filter would not significantly absorb the gas-phase I/SVOCs. Also, there is no obvious difference in signals of Nap products in the case of the dirty filter, suggesting those artifacts could be negligible.

## 2.4 Identification of gas phase 1,2-PhA from m/Q 167

It was mentioned that three isomers of phthalic acid (1,2-PhA, 1,3-PhA and 1,4-PhA) in the gas phase were presented as the  $C_8H_7O_4^+$  signal in the instrument. We were not able to distinguish the three isomers individually. We assumed that the ratios of the isomers in gas phase were the same as that in particle phase. As shown in Table S3, the 1,2-PhA ratio in the particle phase ( $72\% \pm 23\%$ ) was similar to that in Beijing during summer ( $67\% \pm 15\%$ ), but was much higher than that in the PRD region ( $33\% \pm 3\%$ ). This may be explained by the differences in source structure of phthalic acids in the two regions. For example, the higher abundance of 1,4-PhA in particle phase was observed in PRD, which was possibly associated with its widely usage in plastic manufacturing in this region.

The overall uncertainty for gas phase 1,2-PhA was from the uncertainty of measurement precision ( $\pm 15\%$ ), uncertainty of the calibration factor ( $\pm 14\%$ ), uncertainty of wall loss ( $\pm 28\%$ ), and uncertainty of isomer distribution of phthalic acid ( $\pm 30\%$ ). The overall uncertainty for gas phase 1,2-PhA quantification was determined to be 43% through error propagation (Eq S3).

$$UNC_{PhAg} = \sqrt{\sigma_{pre}^2 + \sigma_{cali}^2 + \sigma_{loss}^2 + \sigma_{isomer}^2} \quad (\text{Eq S3})$$

## 3. Uncertainties for particle phase 1,2-PhA measurement.

Quartz filters (Whatman Inc) were used to collect the particle samples. The quartz filters were pre-baked at 550°C beforehand. After collection, the samples were stored under -25°C until analysis was performed. Before the extraction, the quartz filters were spiked with a mixture of deuterated internal recovery standards including 1,2-phthalic acid-*d4*. The samples were then extracted assisted by ultrasonic three times with dichloromethane/methanol (3:1, Sigma-Aldrich Inc). The extracts were filtered and then reduced to about 5 mL using a rotary vacuum evaporator, and further blown to dryness with a mild stream of nitrogen. The concentrated extracts were then split into two fractions. One was derivatized with BSTFA (BSTFA/TMCS, 99:1, Supelco Inc) under 80°C for two hours before GC-MS analysis. An Agilent GC-MS (6890/5973N) equipped with a DB-5MS column (30 m × 0.25 mm I.D.) was used for organic compounds analysis. The oven temperature program was operated as follows: hold 65 °C for 5 min, followed by heating to 300 °C at 10 °C/min, and hold 300 °C for 30 min.

The recovery of 1,2-PhA in filter samples (1,2-PhA<sub>(p)</sub>) was 49±5%, lower than the value 73.1% reported by Zhang et al.<sup>7</sup> and 80.5±7.6% reported by He et al.<sup>8</sup> Several reasons might account for the lower recovery: (1) loss of the target analyte when the extracts were filtered; (2) loss of the target analyte when the near dry extracts were transferred to the derivatizing reaction vial; (3) decomposition of the derivatization products of 1,2-PhA when waiting for the GC-MS injection.

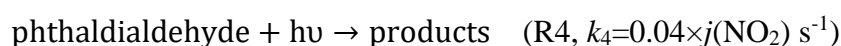
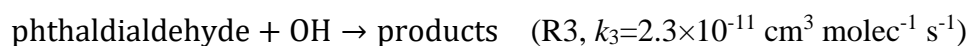
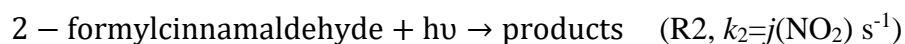
The uncertainty for 1,2-PhA<sub>(p)</sub> determination was attributed to the sampling and measurement uncertainty (Eq S4). The sampling flowrate was calibrated and the uncertainty was within 10%. The measurements of 1,2-PhA<sub>(p)</sub> was interfered by the gas phase phthalic anhydride. In this study, the concentration of phthalic anhydride<sub>(g)</sub> was 3-7 times higher than that of 1,2-PhA<sub>(p)</sub>. It was expected phthalic anhydride<sub>(g)</sub> should contribute up to 10% artifact on 1,2-PhA<sub>(p)</sub> measurement<sup>9</sup>. The pre-processed procedures also influenced the determination of 1,2-PhA<sub>(p)</sub>. The relative error for 1,2-PhA<sub>(p)</sub> determination was estimated to be 40% when considering the sampling and measurement errors.

$$UNC_{PhA_p} = \sqrt{\sigma_{sampling}^2 + \sigma_{measurement}^2} \quad (\text{Eq S4})$$

#### 4. Photolysis of the dicarbonyl products.

The chemical removal processes for 2-FC and phthaldialdehyde in the atmosphere include their further reactions with OH radicals (Reaction R1 and R3) and photolysis (Reaction R2 and R4). Where,  $k_1$  and  $k_3$  are the reaction coefficients for the reaction of OH with 2-FC ( $5.3 \times 10^{-11} \text{ cm}^3 \text{ molec}^{-1} \text{ s}^{-1}$ )<sup>10</sup> and phthaldialdehyde ( $2.3 \times 10^{-11} \text{ cm}^3 \text{ molec}^{-1} \text{ s}^{-1}$ )<sup>11</sup>, respectively.  $k_2$  and  $k_4$  are the photolysis frequencies of 2-FC (equivalent to  $j(\text{NO}_2)$ ,  $\text{s}^{-1}$ ) and phthaldialdehyde ( $0.04 \times j(\text{NO}_2)$ ,  $\text{s}^{-1} \text{ s}^{-1}$ ), obtained from previous laboratory results<sup>10, 11</sup>. The reaction coefficients for 2-FC and OH radical reaction was

twice as that of phthaldialdehyde, while the photolysis frequency for 2-FC was 25 times as that of phthaldialdehyde.



As shown in Figure 3a, the first generation products 2-FC presented a significant peak at noon. Notably phthaldialdehyde also presented a peak at noon, and increased prior to 2-FC. This was contrary to the results from Wang et al.<sup>12</sup> who observed secondary generation of phthaldialdehyde from 2-FC. The fast removal of 2-FC by photolysis could account for this discrepancy, as the loss rate of 2-FC, defined as the product of photolysis frequency and concentration, was 37 times as that of phthaldialdehyde. Upon 2-FC photolysis, phthaldialdehyde started to accumulated so that it increased “first” in atmosphere.

## 5. Contribution of NO<sub>3</sub> pathway to the products formation.

Besides the formation from OH-initiated Nap oxidation, the products also formed from the NO<sub>3</sub>-initiated reactions with Nap during the nighttime<sup>13</sup>. We evaluated the relative importance of Nap oxidation through OH and NO<sub>3</sub> pathway, by comparing the loss rates of Nap by reactions with OH and NO<sub>3</sub> (described in Eq. S5). Where the rate coefficients for Nap reactions with OH ( $k_{\text{Nap+OH}}$ ) and NO<sub>3</sub> ( $k_{\text{Nap+NO}_3}$ ) are  $2.2 \times 10^{-11} \text{ cm}^3$

molec<sup>-1</sup> s<sup>-1</sup> and  $1.2 \times 10^{-13}$  cm<sup>3</sup> molec<sup>-1</sup> s<sup>-1</sup>, respectively. The campaign-average OH concentration in the daytime was  $(1.4 \pm 0.4) \times 10^6$  molec cm<sup>-3</sup>, derived from the empirical function of OH and j(O<sup>1</sup>D)<sup>14</sup>. The concentrations of NO<sub>3</sub> during the night were estimated to be  $(4.2 \pm 0.4) \times 10^7$  molec cm<sup>-3</sup>, when assuming steady state<sup>15</sup> (described in Eq. S6). Note that NO<sub>3</sub> may be overestimated by Eq. S5 due to the heterogeneous losses of NO<sub>3</sub> and N<sub>2</sub>O<sub>5</sub> onto aerosols, which are more significant (69.1-98.8%) for polluted conditions<sup>16</sup>. Thus, the NO<sub>3</sub> concentrations at night were corrected to be  $(1.3 \pm 0.2) \times 10^7$  molec cm<sup>-3</sup>, using the reported losses (~70%) of N<sub>2</sub>O<sub>5</sub> on aerosols.

$$L_{Nap} = k_{Nap+OH}[Nap][OH] + k_{Nap+NO_3}[Nap][NO_3] \quad (\text{Eq. S5})$$

$$[NO_3]_{ss} = \frac{k_{NO_2+O_3}[NO_2][O_3]}{k_{NO_3+NO}[NO] + \sum(k_{NO_3+VOC} \times [VOC]) + J_{NO_3}} \quad (\text{Eq. S6})$$

As shown in Table S4, OH radical reaction is the main pathway for naphthalene during the daytime. The NO<sub>3</sub> pathway plays a minor role (about 8%) for Nap oxidation in the polluted environments.

## 6. OH exposure calculation.

The photochemical-age-based parameterization method was used to calculate the OH exposure (Eq. S7)<sup>17</sup>. In this study, the measured ratio of xylene to toluene was selected to calculate OH exposure ( $[OH]\Delta t$ , molec cm<sup>-3</sup> s). Here, 75% of (C<sub>8</sub>H<sub>10</sub>)H<sup>+</sup> signal measured by PTR-QiTOF was attributed to xylene according to the results from online GC-MS during the campaign.

$$[OH]\Delta t = \frac{1}{k_{Xyl}-k_{Tol}} \times \left( \ln \frac{[Xyl]}{[Tol]} \Big|_{t_0} - \ln \frac{[Xyl]}{[Tol]} \Big|_t \right) \quad (\text{Eq. S7})$$

In Eq S7,  $[OH]$  is the OH radical concentration ( $\text{molec cm}^{-3}$ ), and  $\Delta t$  is the photochemical age (s).  $k_{Xyl}$  and  $k_{Tol}$  are the OH rate constants for xylene (averaged at  $1.63 \times 10^{-11} \text{ cm}^3 \text{ molec}^{-1} \text{ s}^{-1}$ ) and toluene ( $5.63 \times 10^{-12} \text{ cm}^3 \text{ molec}^{-1} \text{ s}^{-1}$ ). It is worth to notice that  $[Xyl]$  is the sum of m,p-xylene and o-xylene, and  $k_{Xyl}$  is calculated as the average value of  $k_{m,p-Xyl}$  ( $1.89 \times 10^{-11} \text{ cm}^3 \text{ molec}^{-1} \text{ s}^{-1}$ ) and  $k_{o-Xyl}$  ( $1.36 \times 10^{-11} \text{ cm}^3 \text{ molec}^{-1} \text{ s}^{-1}$ ).  $\frac{[Xyl]}{[Tol]} \Big|_t$  and  $\frac{Xyl}{Tol} \Big|_{t_0}$  are the mixing ratios of xylene and toluene at t time and in the fresh emissions, respectively.

The determined initial emission ratio of xylene to toluene was  $1.1 \pm 0.4$  ppb/ppb, which was obtained from the data from 2:00 to 4:00 a.m. during the all the haze periods when oxidation processes was weak<sup>18</sup>. Here, the upper limit (1.5 ppb/ppb) of xylene/toluene was used in the OH exposure calculation. The uncertainty for OH exposure calculation mostly arose from selecting the initial emission ratio of xylene/toluene, which would cause an uncertainty about 40%.

## 7. Gas-particle partitioning of 1,2-PhA

### 7.1 Uncertainties for measured $F_p$ .

Upper and lower limits of  $F_p$  were calculated with the mentioned uncertainties in gas phase (43%) and particle phase (40%) 1,2-PhA measurement (Eq. S8 and S9). The upper and lower limit of  $F_p$  were presented in Figure 5.

$$\text{Upper limit} = \frac{1.4 \times \text{PhA}(p)}{1.4 \times \text{PhA}(p) + 0.57 \times \text{PhA}(g)} \quad (\text{Eq. S8})$$

$$\text{Lower limit} = \frac{0.6 \times \text{PhA}(p)}{0.6 \times \text{PhA}(p) + 1.43 \times \text{PhA}(g)} \quad (\text{Eq. S9})$$

## 7.2 Theoretical $F_p$ calculation

The theoretical  $F_p$  of 1,2-PhA was predicted by the absorption partitioning model (Eq. S10). The effective saturation mass concentration  $C^*$  ( $\mu\text{g}/\text{m}^3$ ) has been considered as a key factor to influence the modelled  $F_p$ .  $C^*$  is proportional to the saturated vapor pressure ( $P_v$ , Pa) as shown in Eq. S11, where  $M$  is the molecular weight ( $\text{g mol}^{-1}$ ),  $\zeta$  is the activity coefficient in aerosol phase,  $R$  is the gas constant ( $8.314 \text{ J mol}^{-1} \text{ K}^{-1}$ ) and  $T$  is the temperature (K). In this work,  $P_v$  at the campaign-average temperature of 275 K was derived from the multiphase system online property prediction tool developed by University of Manchester (UManSysProp, <http://umansysprop.seaes.manchester.ac.uk>), which provides several empirical  $P_v$  estimation approaches such as Nannoolal (2008), Myrdal and Yalkowsky (1997) and Compernelle (2011), abbreviated to NN, MY and CP.

$$F_p = \left(1 + \frac{C^*}{OA}\right)^{-1} \quad (\text{Eq. S10})$$

$$C^* = \frac{M10^6 \zeta P_V}{760RT} \quad (\text{Eq. S11})$$

### 7.3 Comparison of the observed and theoretical $C^*$

The observed  $C^*$  was estimated by using the measured OA from Q-ACSM and the mass concentrations of 1,2-PhA in gas- and particle-phase (Eq. S12). The observed and theoretical  $C^*$  for 1,2-PhA were performed in Figure S13. The observed  $C^*$  of 1,2-PhA was estimated to be  $27 \pm 21 \mu\text{g}/\text{m}^3$  and gradually grew over the pollution episode. In contrast, the values of the theoretical  $C^*$  by UManSysProp using the NN, MY and CP method were 0.07, 4.18 and  $0.02 \mu\text{g}/\text{m}^3$ , respectively, when the activity coefficient was set to 1. The activity coefficient was also chosen to be 0.3 and 3 to represent the lower and upper limits of the theoretical  $C^*$ <sup>19</sup>. Barley et al. (2010) proposed that the NN method was more accurate for  $P_V$  prediction as a larger size of training set with thousands of compounds was used<sup>20, 21</sup>. In this study, the observed  $C^*$  of 1,2-PhA was found to be 1–3 orders of magnitude larger than theoretical calculations. Conservatively, the observed  $C^*$  was still 3–5 times higher than the MY approach when the uncertainties of  $C^*$  estimation were considered. The measured ratios of 1,2-PhA<sub>(g)</sub> to 1,2-PhA<sub>(p)</sub> fluctuated between 0.2 and 0.9, generally agreed with the range in early field campaigns (1.0–5.0)<sup>22</sup>, while the campaign-average OA mass was as high as  $70 \mu\text{g}/\text{m}^3$ , about 20–30 times higher than previous field results ( $2.3\text{--}3.7 \mu\text{g}/\text{m}^3$ )<sup>22, 23</sup>. It indicates that the pronounced increase of OA during the haze events would play a key role in affecting the volatility and phase partitioning of 1,2-PhA.

$$C^* = OA \times \frac{C_{gas}}{C_{particle}} \quad (\text{Eq. S12})$$

## 8. Formation of 1,2-PhA(p) through dissolution

In addition to partitioning to organic aerosol, Henry's law was used to predict the concentration of 1,2-PhA dissolved in the aqueous phase ( $C_{aq}$  in Eq. S13), where  $H_{cp,i}$  is the Henry solubility ( $\text{mol m}^{-3} \text{ Pa}^{-1}$ ) which can be obtained from literatures<sup>24</sup>.  $p_i$  is the partial pressure of phthalic anhydride or 1,2-PhA in the gas phase. The aerosol water content (AWC) was calculated using the ISORROPIA-II thermodynamic equilibrium model with the measured RH and aerosol inorganic composition ( $\text{Na}^+$ ,  $\text{NH}_4^+$ ,  $\text{Ca}^{2+}$ ,  $\text{K}^+$ ,  $\text{Mg}^{2+}$ ,  $\text{SO}_4^{2-}$ ,  $\text{NO}_3^-$  and  $\text{Cl}^-$ )<sup>25, 26</sup>. It was assumed that phthalic anhydride dissolved in aerosol water would convert to 1,2-PhA completely. The ionization equilibrium of aqueous phase 1,2-PhA was not considered in this study. The predicted 1,2-PhA dissolved in aerosol water ranged 0.001 to 0.008  $\mu\text{g}/\text{m}^3$ , and increased with AWC. The dissolution pathway contributed less than 10% to the total 1,2-PhA<sub>(p)</sub> formation (Figure S14).

$$c_{aq} = \sum_i^n H_{cp,i} \times p_i \quad (\text{Eq. S13})$$

## 9. Aerosol pH estimation

In this study, the aerosol pH was calculated by using the ISORROPIA-II model and the online measurements of RH and PM<sub>2.5</sub> composition ( $\text{Na}^+$ ,  $\text{NH}_4^+$ ,  $\text{Ca}^{2+}$ ,  $\text{K}^+$ ,  $\text{Mg}^{2+}$ ,  $\text{SO}_4^{2-}$ ,  $\text{NO}_3^-$  and  $\text{Cl}^-$ )<sup>26</sup>. And the concentrations of gaseous  $\text{NH}_3$  were taken from the observation results from the same campaign<sup>27</sup>. Briefly, ammonium, nitrate and sulfate

were the major ions in  $PM_{2.5}$ . The equivalent ratio was calculated to 0.99 for the measured cation and anion ions. The forward mode was used for pH prediction, and the aerosol was assumed as metastable under high RH conditions ( $56\% \pm 11\%$ ). The average pH in aerosol water was  $4.0 \pm 0.2$  and  $4.3 \pm 0.3$  for Haze1 and Haze2 (Figure S14), respectively. This result was in good agreement with recent study by Liu et al<sup>27</sup>.

## 10. Estimated SOA formation from mono-aromatics and PAHs

### 10.1 Tracer product-based method

1,2-PhA was a tracer product for the SOA from Nap and MN oxidation based on chamber experiments. The SOA produced from 2-ring PAHs ( $SOA_{Nap+MN}$ ) could be derived from 1,2-PhA<sub>(p)</sub> ( $PhA_{mea}$ ,  $\mu\text{g}/\text{m}^3$ ) measured in ambient samples and the mass fractions of 1,2-PhA<sub>(p)</sub> founded in PAH SOA in chamber studies, as proposed by Kleindienst et al (Eq. S14)<sup>9</sup>. However, the experimental high- $\text{NO}_x$  conditions (e.g., precursor and  $\text{NO}_x$  concentrations) in previous chamber studies differed with the haze conditions in this field campaign (Table S5). The Nap concentrations in chamber experiments were usually 1–3 orders of magnitude higher than real atmosphere. Although the  $\text{NO}_x$  concentrations in chamber were comparable to the observed  $\text{NO}_x$  in haze episodes, the ratios of Nap/ $\text{NO}_x$  in laboratories were much higher, which indicates that more abundant  $\text{NO}_x$  encountered during the haze episodes in Beijing. However, the effect of  $\text{NO}_x$  levels on the mass fraction of 1,2-PhA<sub>(p)</sub> ( $f_{\text{SOA}}$ ) in Nap-SOA is still under

discussion. The chamber experiments by Kleindienst et al.<sup>9</sup> indicate that the  $f_{SOA}$  of 1,2-PhA<sub>(p)</sub> seemed to be almost stable at 2.0% for both in the presence and absence of NO<sub>x</sub>. But, Kautzman et al.<sup>28</sup> found higher  $f_{SOA}$  of 1,2-PhA<sub>(p)</sub> under low- NO<sub>x</sub> (4.9±0.2%) than high- NO<sub>x</sub> conditions (2.7±0.9%).

Given the possible NO<sub>x</sub> effect on  $f_{SOA}$ , we chose the lower limit of  $f_{SOA}$  (2%) in Nap-SOA for subsequent calculations. In addition, 1,2-PhA<sub>(p)</sub> is also a tracer product of MN under high-NO<sub>x</sub>, with its  $f_{SOA}$  of 1.6±0.9%. So, in this study, a weighted-average  $f_{SOA}$  of 1,2-PhA<sub>(p)</sub> was determined to be 1.9%, scaled by the fractions of Nap (80%) and MN (20%) during the campaign. Due to the different conditions between laboratories and field study, we estimated an overall uncertainty of 50% on  $f_{SOA}$ .

$$SOA_{Nap+MN} = \frac{PhA_{mea} - PhA_{pri}}{f_{SOA}} \quad (\text{Eq. S14})$$

$$PhA_{pri} = \sum_i^n PM_{2.5} \times source\ contribution_i \times EF_i \quad (\text{Eq. S15})$$

Primary 1,2-PhA<sub>(p)</sub> ( $PhA_{pri}$ , μg/m<sup>3</sup>) could positively bias SOA<sub>Nap+MN</sub> calculation. Primary sources of 1,2-PhA<sub>(p)</sub> include vehicle exhaust, coal combustion, and biomass burning.  $PhA_{pri}$  can be roughly estimated by Eq. S15, using emission factors of 1,2-PhA<sub>(p)</sub> for major combustion sources ( $EF_i$ , μg PhA μg<sup>-1</sup> PM<sub>2.5</sub>), measured PM<sub>2.5</sub> (μg/m<sup>3</sup>) and source contributions for ambient PM<sub>2.5</sub>. The 1,2-PhA<sub>(p)</sub> emission factor was 4.0×10<sup>-4</sup> μg/μg PM<sub>2.5</sub> for vehicle exhaust, 2.4×10<sup>-4</sup> μg/μg PM<sub>2.5</sub> for coal combustion, and 2.1×10<sup>-4</sup> μg/μg PM<sub>2.5</sub> for biomass burning<sup>7, 29-31</sup>. Source apportionment result of

ambient PM<sub>2.5</sub> was taken during the heating season in Beijing (Table S6)<sup>32</sup>. Based on Eq. S15, vehicle exhaust, coal combustion and biomass burning could emit  $5.1 \times 10^{-5}$ ,  $6.0 \times 10^{-5}$  and  $2.3 \times 10^{-5}$   $\mu\text{g}$  1,2-PhA<sub>(p)</sub> per  $\mu\text{g}$  PM<sub>2.5</sub> in ambient air, which accounted for 44%, 39% and 17% of the primary 1,2-PhA<sub>(p)</sub> respectively. The calculated primary 1,2-PhA<sub>(p)</sub> ranged from 0.022 to 0.044  $\mu\text{g}/\text{m}^3$ , and occupied a larger fraction of total 1,2-PhA<sub>(p)</sub> during the period of Haze2 than Haze1 (Table S7). Estimated SOA formation from Nap and MN by tracer product-based method in Haze1 and Haze2 was summarized in Table S8.

In this method, determination of primary 1,2-PhA<sub>(p)</sub> and the mass fraction of 1,2-PhA<sub>(p)</sub> is one of the key factors influencing SOA estimation. The uncertainty in primary 1,2-PhA<sub>(p)</sub> was relatively large, depending on the error in source apportionment of ambient PM<sub>2.5</sub>. The error for the primary 1,2-PhA<sub>(p)</sub> estimation was assumed to be 50%. Mass fraction of 1,2-PhA<sub>(p)</sub> was obtained from laboratory studies. The uncertainty of the laboratory obtained mass fraction of 1,2-PhA<sub>(p)</sub> was estimated to be 50%. Therefore, the uncertainty of the estimated SOA formation by the tracer product-based method was calculated as 81% through error propagation (Eq. S16), when considering the uncertainty from total 1,2-PhA<sub>(p)</sub> measurement (40%), mass fraction in SOA (50%), and the primary 1,2-PhA<sub>(p)</sub> estimation (50%).

$$Unc_{SOA,tracer} = \sqrt{\sigma_{mea}^2 + \sigma_{fraction}^2 + \sigma_{pri}^2} \quad (\text{Eq. S16})$$

## 10.2 Precursor consumption-based method

The contributions of Nap, MN, and mono-aromatics oxidation to SOA formation were also calculated by the product of the consumed concentrations of precursors relative to CO ( $\frac{\Delta VOC}{\Delta CO}_i$ ) and their SOA yield (Eq S17 and Eq S18)<sup>18, 33</sup>.

$$\left. \frac{\Delta VOC}{\Delta CO} \right|_i = ER_i \times (1 - \exp(-k_i [OH] \Delta t)) \quad (\text{Eq. S17})$$

$$\frac{\Delta SOA}{\Delta CO}_{cal} = \sum_i^n \left. \frac{\Delta VOC}{\Delta CO} \right|_i \times Yield_i \quad (\text{Eq. S18})$$

Where  $ER_i$  is the emission ratio of VOCs and IVOCs relative to CO in the unit of  $\mu\text{g m}^{-3} \text{ppm}^{-1} \text{CO}$ , which was obtained from the linear-regression slope of VOCs/IVOCs versus CO from 2:00-4:00 a.m.  $k_i$  is the rate constant of VOCs/IVOCs with OH radical ( $\text{cm}^3 \text{molec}^{-1} \text{s}^{-1}$ ).  $\frac{\Delta SOA}{\Delta CO}_{cal}$  is the calculated SOA formation from VOCs/IVOCs per unit CO in the unit of  $\mu\text{g m}^{-3} \text{ppm}^{-1} \text{CO}$ .  $Yield_i$  is SOA production yield for each precursor determined from previous chamber studies. The emission ratios, SOA yield of mono-aromatics, Nap and MN are summarized in Table S9, and the calculated SOA formation during the haze period is shown in Figure S16.

SOA yields of VOCs under high- $\text{NO}_x$  can be expressed as an empirical function of OA mass loadings based on the two-product model<sup>34</sup>. Here, SOA yields for VOCs and IVOCs were extrapolated to high OA conditions ( $70 \mu\text{g/m}^3$ ). The yields are also influenced by ambient temperature, then such an effect is corrected with the Clausius-Clapeyron equation at the temperature of 275K<sup>35</sup>. In addition, the effect of wall loss on

SOA yields in chamber experiments are also considered according to Zhang et al. (2014)<sup>36</sup>.

The uncertainty for this method is determined by chemical consumption and SOA yields of the precursors. The uncertainties in chemical consumption of precursors are related to  $ER_i$  and OH exposure calculation, and the corresponding RSD was 5% and 40%, respectively. The uncertainties of SOA yields were estimated to be 10-25%. Considering the RSD of  $ER_i$  (5%), OH exposure calculation (40%), and SOA yields (10-25%), a total uncertainty was estimated to be 47% by the precursor consumption-based method (Eq. S19).

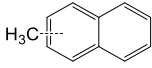
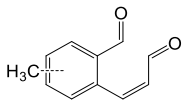
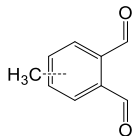
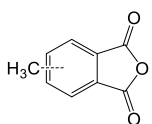
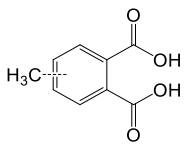
$$Unc_{SOA,precursor} = \sqrt{\sigma_{ER}^2 + \sigma_{OH\Delta t}^2 + \sigma_{Yield}^2} \quad (\text{Eq. S19})$$

### 10.3 Estimated SOA fraction in organic aerosol

The calculated SOA from Nap, MN, and mono-aromatics oxidation by the tracer product-based method and the precursor consumption-based method were then compared with the measured OA mass concentration in  $PM_{2.5}$  by ACSM. The SOA fraction was reported to be about 30%-50% of the measured OA (in  $PM_1$ ) in winter Beijing determined from Aerosol Mass Spectrometer (AMS) or ACSM measurements (Table S10)<sup>37-39</sup>, and showed an increasing trend in recent years. Assuming that SOA primarily existed in  $PM_1$  and the  $PM_1/PM_{2.5}$  ratio was 0.9<sup>40</sup>, then SOA fraction in the

OA of  $PM_{2.5}$  was nearly 40%. Thus, we estimated 40% of OA mass concentration was contributed from SOA at noon.

Table S1. Information of MN and its gas-phase oxidation products observed by PTR-QiTOF

Compound	Formula	$[M+H]^+$	Phase	PTR Sensitivity, Detection		Proposed
			Distribution	ncps/ppb	Limit, ppt	Structure
Methylnaphthalene	$C_{11}H_{10}$	143.0855	g	3383 <sup>a</sup>	7	
Methyl-formylcinnamaldehyde	$C_{11}H_{10}O_2$	175.0753	g, p	4862 <sup>a</sup>	5	
Methyl-phthaldialdehyde	$C_9H_8O_2$	149.0597	g	4313 <sup>a</sup>	3	
Methyl-phthalic anhydride	$C_9H_6O_3$	163.039	g	4614 <sup>a</sup>	4	
1,2-Methyl-phthalic acid	$C_9H_8O_4$	181.0495	g, p	3488 <sup>a</sup>	3	

<sup>a</sup>Sensitivity was estimated from compounds with similar structure or molecular weight.

Table S2. Determination of the wall losses for the oxidation products with ambient air.

Number of test	Relative deviation, %			
	2-FC	phthaldialdehyde	Anhydride	PhA
1	-17.7	-10.0	3.1	-8.4
2	-42.2	-10.0	-4.6	-
3	-9.2	-29.1	-9.6	-41.5
4	-12.8	-12.6	-1.5	-35.5
5	-0.6	-3.8	-2.3	-5.6
6	-	-12.7	-9.5	-32.4
7	-3.3	-17.4	-1.6	-28.0
8	-17.7	-	-5.0	-1.7
Average	-14.8	-13.7	-3.9	-21.9
S.D.	13.7	7.9	4.3	16.2

Table S3. Average concentration of the particle phase phthalic acid isomers (1,2-PhA, 1,3-PhA and 1,4-PhA) during the Haze period from Dec 17 to Dec 21.

1,2-PhA, $\mu\text{g}/\text{m}^3$	1,3-PhA, $\mu\text{g}/\text{m}^3$	1,4-PhA, $\mu\text{g}/\text{m}^3$	F <sub>1,2-PhA</sub> , %	Reference
0.103±0.043	-	0.040±0.018	72±23	This study
0.078±0.018	0.005±0.001	0.032±0.011	67±15	Beijing, summer, 2006 <sup>a</sup>
0.013±0.007	0.001±0.001	0.023±0.009	33±3	PRD, annual, 2012 <sup>b</sup>
0.003±0.001	0.001±0.001	0.006±0.001	35±20	Iowa, winter, 2015 <sup>c</sup>

Data sources: (a) Ho et al., 2010<sup>41</sup>, (b) He et al., 2018<sup>8</sup>, (c) Ibrahim et al., 2016<sup>22</sup>

Table S4. Rate coefficients, oxidant concentrations and loss rates of Nap during daytime and nighttime in the haze episodes

Oxidant	Rate coefficients, $\text{cm}^3 \text{ molec}^{-1} \text{ s}^{-1}$	Concentration of oxidant, $\text{molec cm}^{-3}$		Loss rate of Nap, ppt/h	
		Daytime	Nighttime	Daytime	Nighttime
OH	$2.2 \times 10^{-11}$	$(1.4 \pm 0.4) \times 10^6$	-	$21.9 \pm 8.9$	-
NO <sub>3</sub>	$1.2 \times 10^{-13}$	$(2.2 \pm 1.2) \times 10^4$	$(1.3 \pm 0.2) \times 10^7$	-	$1.9 \pm 0.3$

Table S5. The high-NO<sub>x</sub> conditions and  $f_{\text{SOA}}$  of 1,2-PhA<sub>(p)</sub> from photooxidation of Nap and MN in chamber studies, compared with haze conditions in the winter campaign

	Precursor, (ppb)	NO <sub>x</sub> , (ppb)	VOC/NO <sub>x</sub> , (ppb/ppb)	$f_{\text{SOA}}$ , (%)	Reference
Naphthalene: high-NO <sub>x</sub>					
Laboratory	20–240	111–281	0.1–2.2	2.0±0.8	Kleindienst et al. <sup>9</sup>
Laboratory	30–48	166–289	0.1–0.3	2.7±0.9	Kautzman et al. <sup>28</sup>
Haze events	0.21-0.72	74-243	<0.006	-	this study
Methyl-naphthalene: high-NO <sub>x</sub>					
Laboratory	74–86	180–299	0.3–0.5	1.6±0.9	Kleindienst et al. <sup>9</sup>
Haze events	0.03–0.24	74–236	<0.002	-	this study

Table S6. Emission factors of 1,2-PhA in PM<sub>2.5</sub> from primary anthropogenic sources

Sources	Contributions to PM <sub>2.5</sub> <sup>a</sup> , %	EF <sub>PhA</sub> , ×10 <sup>-4</sup> μg PhA μg <sup>-1</sup> PM <sub>2.5</sub>
Coal combustion	21.7	2.4
Traffic related	14.9	4.0
Biomass burning	11.2	2.1

<sup>a</sup>The contributions of primary anthropogenic sources to ambient PM<sub>2.5</sub> were from Yang et al.<sup>32</sup>, and were assumed to be constant for Haze1 and Haze2 even though sources might change from Haze1 to Haze2.

Table S7 Estimation of primary and secondary 1,2-PhA in ambient PM<sub>2.5</sub> samples during haze periods.

Period	Date	PhA <sub>mea</sub> , $\mu\text{g}/\text{m}^3$	PhA <sub>pri</sub> , $\mu\text{g}/\text{m}^3$	PhA <sub>sec</sub> , $\mu\text{g}/\text{m}^3$
Haze1	Dec 17	0.15	0.02	0.13
	Dec 18	0.13	0.03	0.10
	Dec 19	0.12	0.03	0.09
Haze2	Dec 20	0.07	0.04	0.03
	Dec 21	0.05	0.04	0.00

Table S8. SOA formation from Nap and MN by tracer product-based method in Haze1 and Haze2.

Period	Date	SOA <sub>Nap+MN</sub> , $\mu\text{g}/\text{m}^3$	Explained SOA, %
Haze1	Dec 17	6.8	32.3
	Dec 18	5.2	21.9
	Dec 19	4.6	15.2
Haze2	Dec 20	1.6	4.6
	Dec 21	0.1	0.3
Haze1&2	average $\pm$ s.d.	3.7 $\pm$ 2.7	14.9 $\pm$ 13.0

Table S9. Emission ratio (ER), SOA yield (at OA=70 $\mu\text{g}/\text{m}^3$ ) and SOA formation relative to CO from mono-aromatics, Nap and MN estimated by the precursor consumption-based method.

Precursors	ER, ppb/ppm CO	SOA yield*, % (OA=70 $\mu\text{g}/\text{m}^3$ )	Calculated SOA , $\mu\text{g}/\text{m}^3/\text{ppm CO}$	Explained SOA, %
Benzene	0.66 $\pm$ 0.02	82.5	0.13 $\pm$ 0.03	1.98 $\pm$ 0.37
Toluene	0.60 $\pm$ 0.02	18.1	0.12 $\pm$ 0.03	1.91 $\pm$ 0.32
C8 aromatics	1.19 $\pm$ 0.05	21.3	0.64 $\pm$ 0.10	9.81 $\pm$ 1.35
C9 aromatics	0.22 $\pm$ 0.01	21.5	0.18 $\pm$ 0.02	2.77 $\pm$ 0.36
Naphthalene	0.14 $\pm$ 0.01	82.3	0.49 $\pm$ 0.06	7.64 $\pm$ 0.99
Methylnaphthalene	0.04 $\pm$ 0.00	63.8	0.16 $\pm$ 0.01	2.56 $\pm$ 0.36

\*SOA yields for benzene and toluene were obtained from Ng et al. (2007)<sup>42</sup>, C8 and C9 aromatics were from Li et al. (2016)<sup>43</sup>, and Nap and MN were from Chan et al. (2009)<sup>44</sup>.

Table S10. Reported SOA fraction in organic aerosol in winter Beijing

Sampling Site	Instrument	Data	SOA, $\mu\text{g}/\text{m}^3$	OA, $\mu\text{g}/\text{m}^3$	Fraction, %	Reference
PEK	HR-AMS <sup>a</sup>	Nov, 2010	11	35	30	Hu et al., 2016 <sup>45</sup>
IAP	ACSM <sup>a</sup>	Nov, 2012	11	34	32	Sun et al., 2012 <sup>46</sup>
IAP	HR-AMS <sup>a</sup>	Jan, 2013	27	51	52	Zhang et al., 2014 <sup>37</sup>
IAP	HR-AMS <sup>a</sup>	Dec, 2013	17	38	43	Sun et al., 2016 <sup>39</sup>
IAP	HR-AMS <sup>a</sup>	Jan, 2014	14	27	52	Zhang et al., 2015 <sup>47</sup>
PEK	HR-AMS <sup>a</sup>	Jan, 2016	12	27	46	Zheng et al., 2016

Sampling sites: Peking University (PEK); Institute of Atmospheric Physics (IAP).

<sup>a</sup> PM<sub>1</sub> was measured by the instrument.

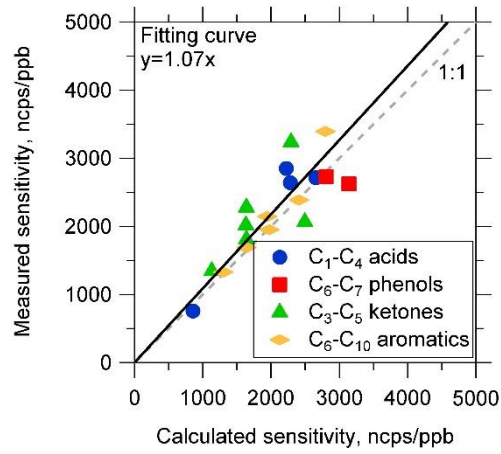


Figure S1. Comparison of the theoretical and measured calibration factors for several kinds of compounds.

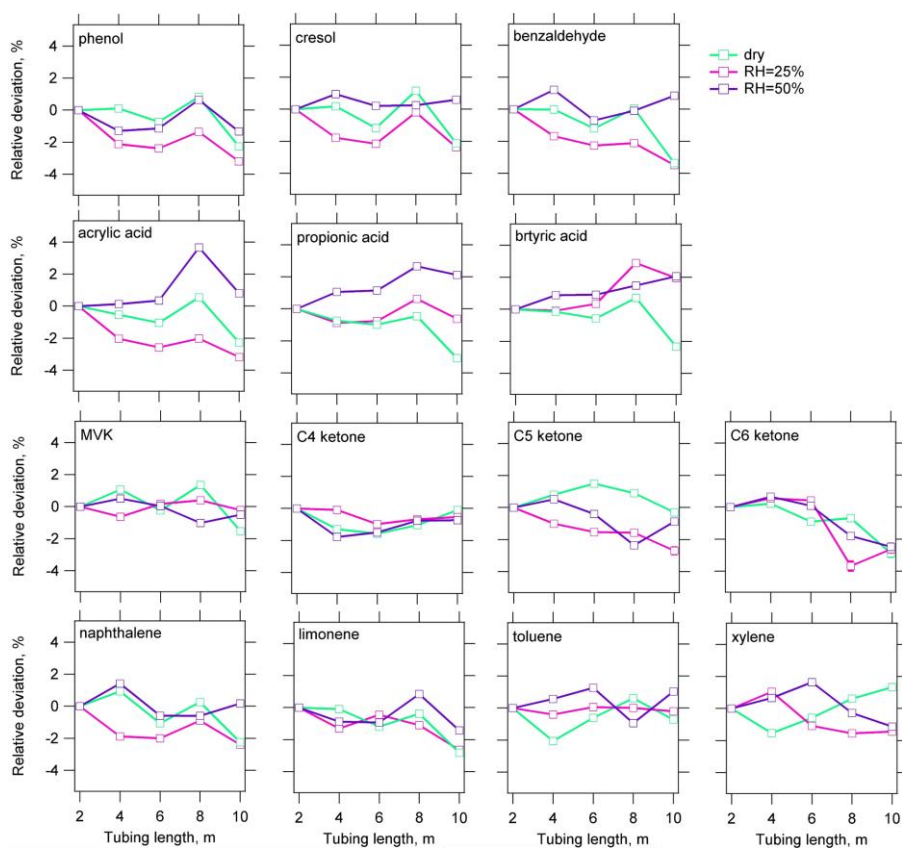


Figure S2. Effect of tubing length and RH on the losses of several kinds of compounds.

The maximum and minimum value of the y-axis represented the measurement precision of the instrument.

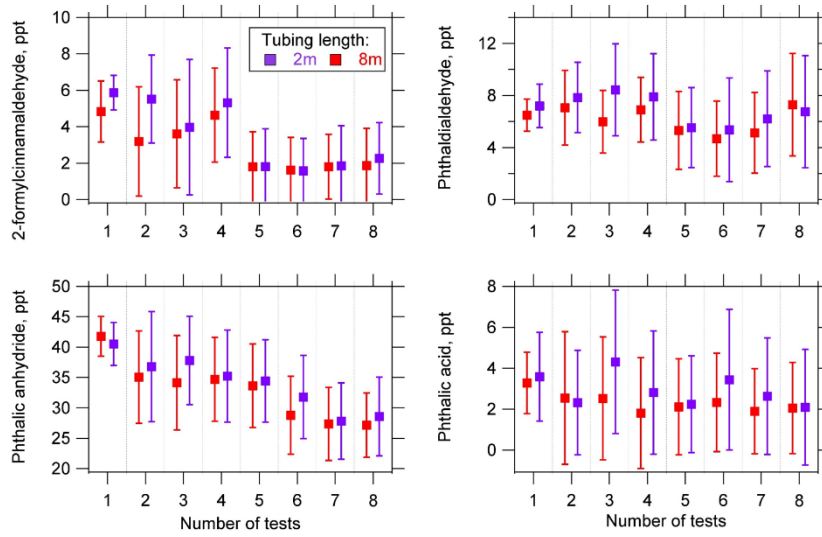


Figure S3. Comparison of the mixing ratios of the oxidation products with 2 m-long and 8 m-long Teflon tubing in the wall loss tests.

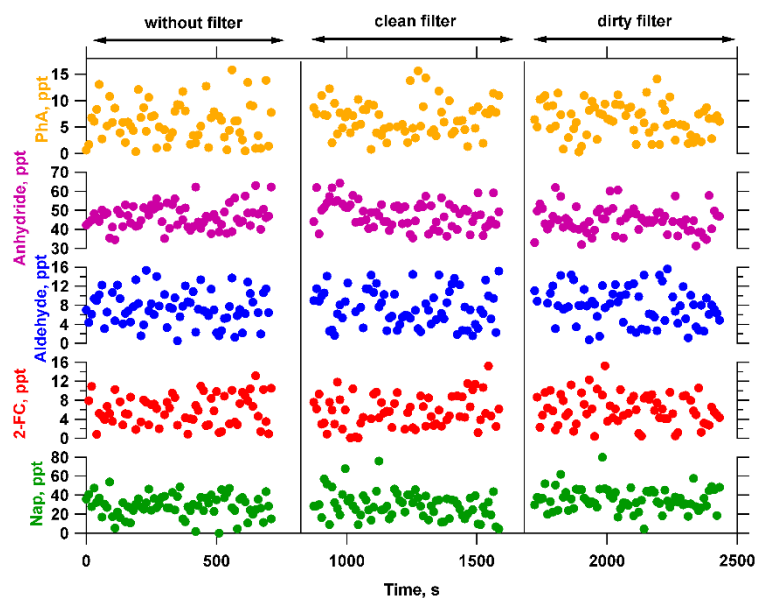


Figure S4. Examining the effect of gas absorption and particle re-evaporation on the quantification of the target compounds. Nap=naphthalene; 2-FC=2-formylcinnamaldehyde; Aldehyde=phthaldialdehyde; Anhydride=phthalic anhydride; PhA=phthalic acid.

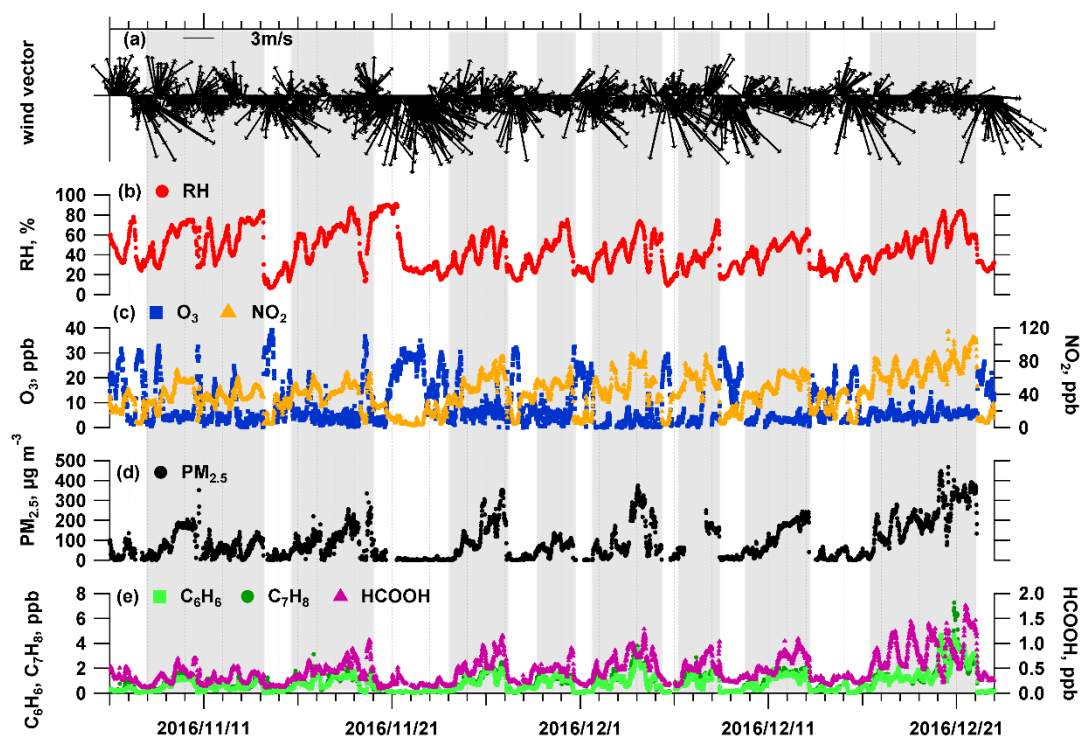


Figure S5. Time series of PM<sub>2.5</sub>, tracer gases (O<sub>3</sub>, NO<sub>2</sub> and CO), benzene (C<sub>6</sub>H<sub>6</sub>), toluene (C<sub>7</sub>H<sub>8</sub>), formic acid (HCOOH), and metrological parameters (wind vector and RH) during the whole campaign. Haze periods are presented in grey shaded area.

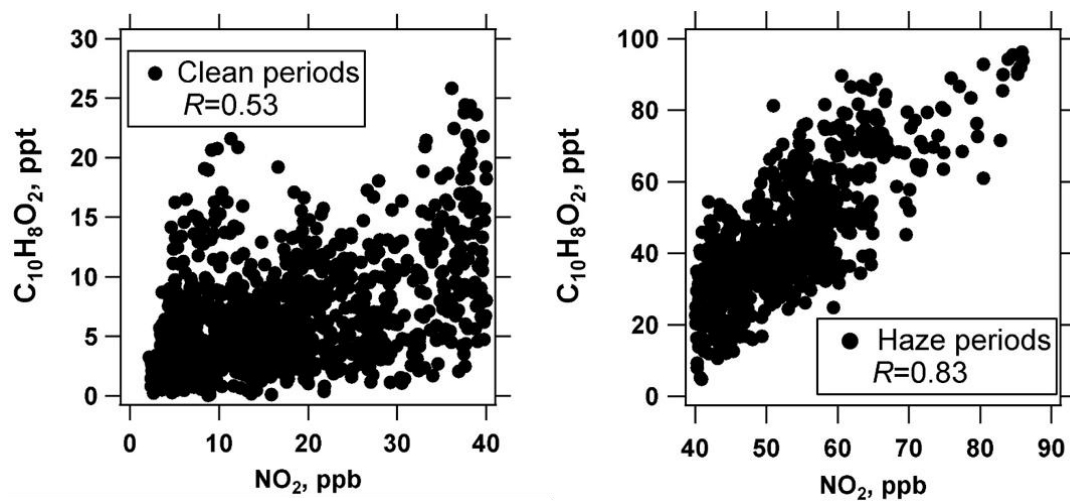


Figure S6. Scatterplot of 2-formylcinnamaldehyde versus NO<sub>2</sub> during all the clean periods (left panel) and haze periods (right panel).

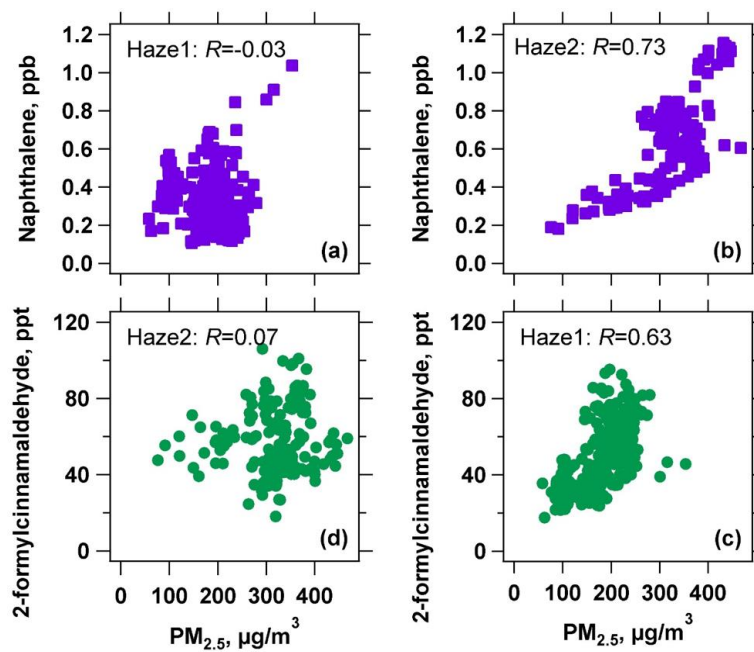


Figure S7. Scatterplots of Nap versus PM<sub>2.5</sub> during (a) Haze1 and (b) Haze2, and scatterplot of 2-formylcinnamaldehyde versus PM<sub>2.5</sub> during (c) Haze1 and (d) Haze2.

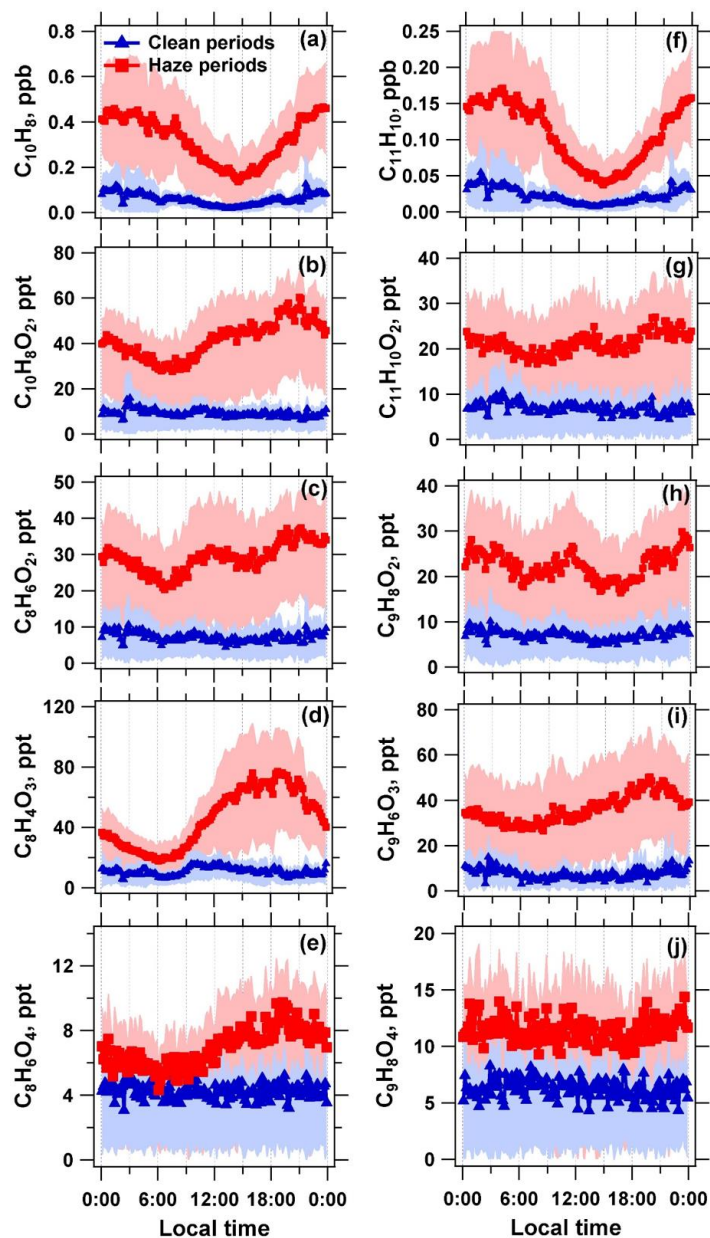


Figure S8. Diurnal patterns of Nap, MN, and their oxidation products during all the haze periods (red squares) and clean periods (blue triangles), respectively. Left column are Nap (a) and its oxidation products (b, c, d, e); Right column are MN (f) and its oxidation products (g, h, i, j). Light red and light blue shades represent the error bars of

1σ.

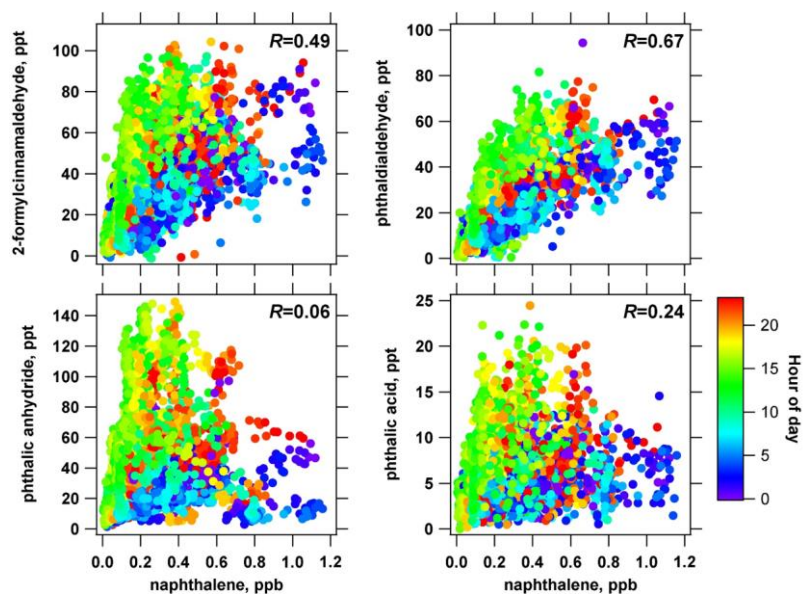


Figure S9. Scatterplots of gas-phase products versus Nap during all haze events.

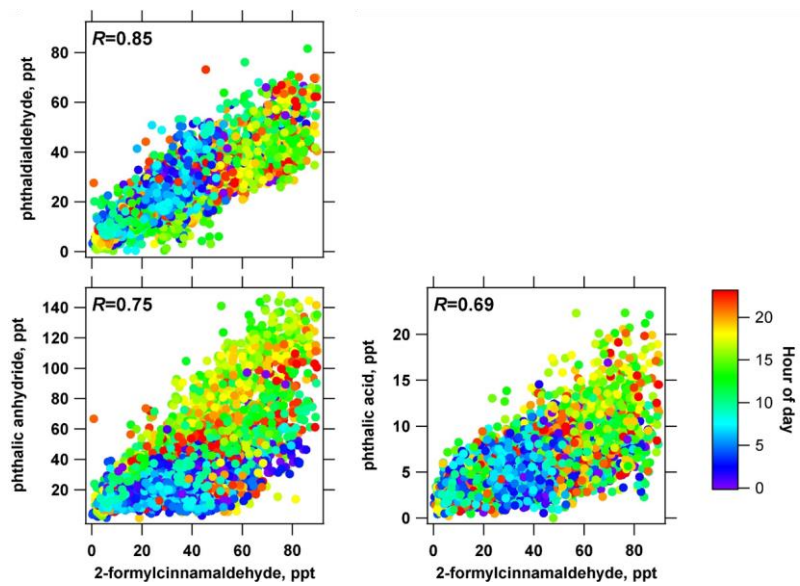


Figure S10. Correlations among the ring-opening Nap products during all haze events.

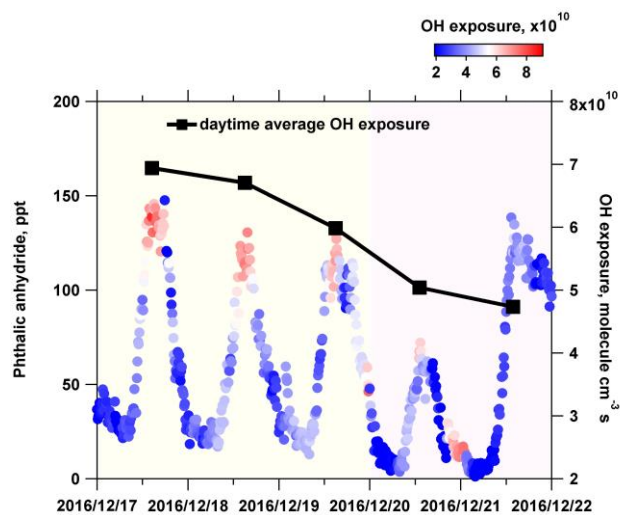


Figure S11. Time series of phthalic anhydride from Dec 17 to Dec 21 (dots), and the makers were colored by the calculated OH exposure. Black squares represent the trends of daytime-average OH exposure (10:00 a.m. to 4:00 p.m.).

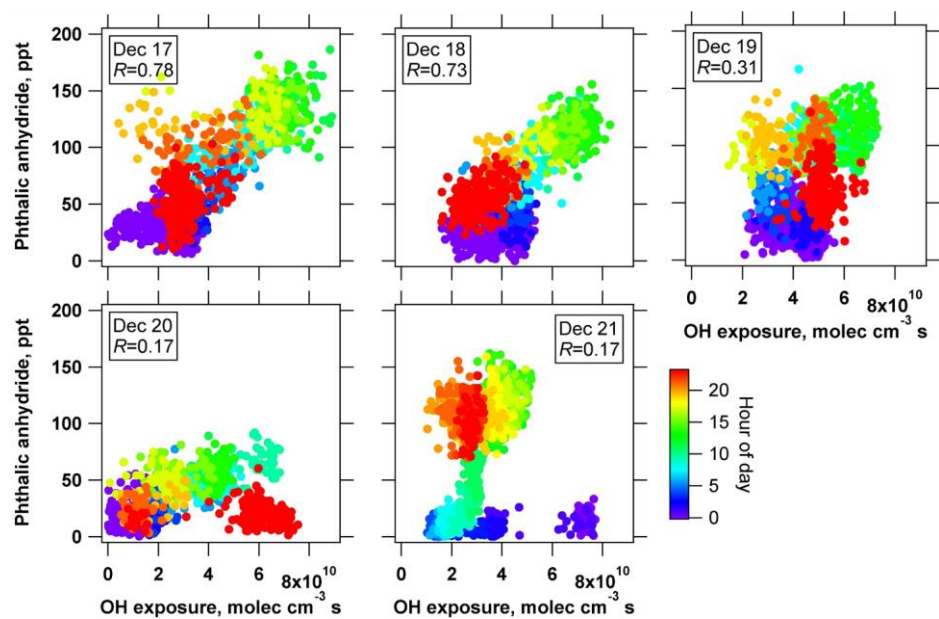


Figure S12. Day-to-day scatterplots of phthalic anhydride and OH exposure during the haze episodes from Dec 17 to Dec 21 (color-coded by the hour of the day).

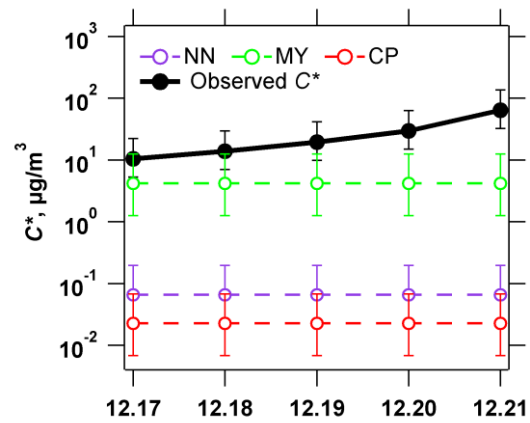


Figure S13. Comparison between the observed  $C^*$  and the theoretical values for 1,2-PhA. Error bars represent the upper and lower limits of  $C^*$ .

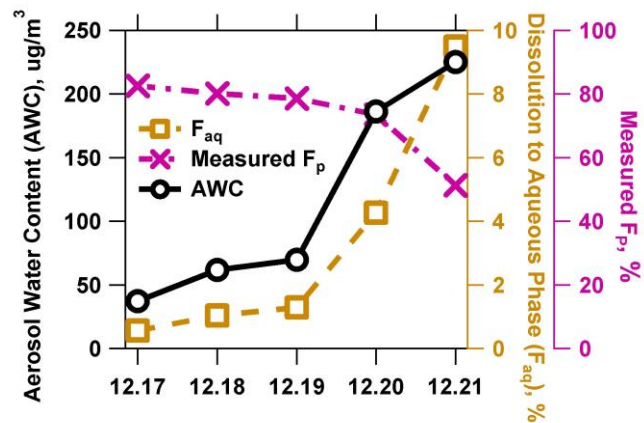


Figure S14. Variation of dissolved 1,2-PhA in aqueous phase ( $F_{aq}$ ) with aerosol water content (AWC) from Dec 17 to Dec 21.

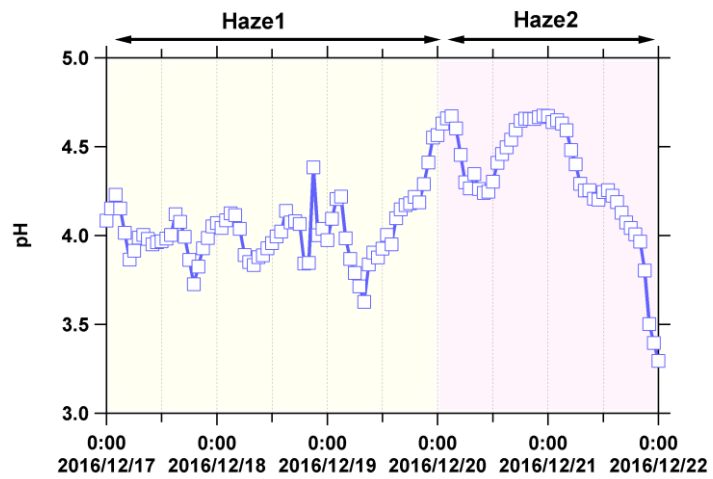


Figure S15. The calculated aerosol pH during the haze period from Dec 17 to Dec 21.

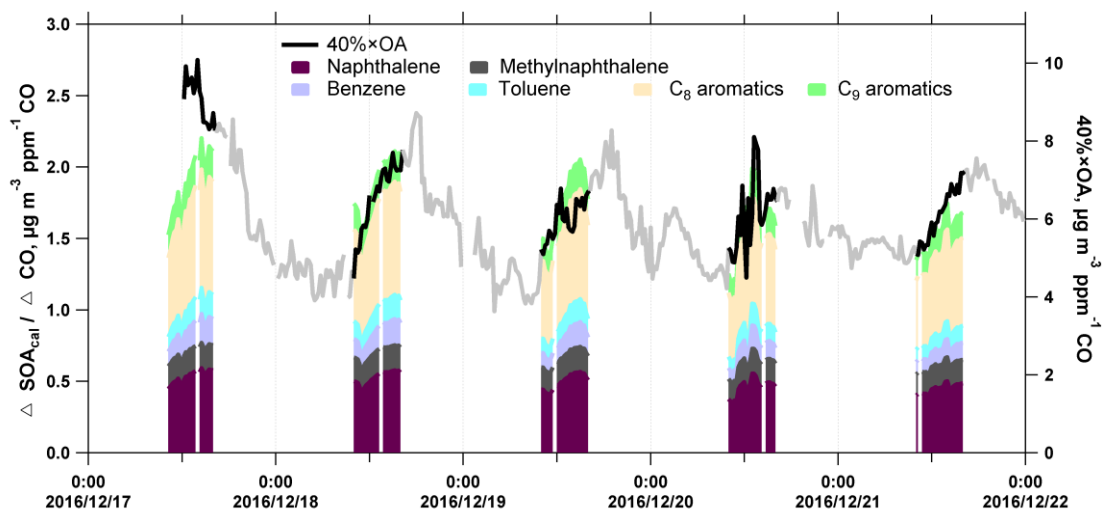


Figure S16. Estimation of daytime SOA formation from Nap, MN, and mono-aromatics oxidation by the precursor consumption-based method from Dec 17 to Dec 21. The grey line represents measured OA is influenced by POA at that time.

## REFERENCE

1. de Gouw, J. A.; Goldan, P. D.; Warneke, C.; Kuster, W. C.; Roberts, J. M.; Marchewka, M.; Bertman, S. B.; Pszenny, A. A. P.; Keene, W. C., Validation of proton transfer reaction-mass spectrometry (PTR-MS) measurements of gas-phase organic compounds in the atmosphere during the New England Air Quality Study (NEAQS) in 2002. *Journal of Geophysical Research-Atmospheres* 2003, 108, D21, 4682, doi: 10.1029/2003jd003863.
2. Chernushevich, I. V.; Loboda, A. V.; Thomson, B. A., An introduction to quadrupole-time-of-flight mass spectrometry. *Journal of Mass Spectrometry* 2001, 36, (8), 849-865.
3. Taipale, R.; Ruuskanen, T. M.; Rinne, J.; Kajos, M. K.; Hakola, H.; Pohja, T.; Kulmala, M., Technical Note: Quantitative long-term measurements of VOC concentrations by PTR-MS - measurement, calibration, and volume mixing ratio calculation methods. *Atmospheric Chemistry and Physics* 2008, 8, (22), 6681-6698.
4. Hayward, S.; Hewitt, C. N.; Sartin, J. H.; Owen, S. M., Performance characteristics and applications of a proton transfer reaction-mass spectrometer for measuring volatile organic compounds in ambient air. *Environmental Science & Technology* 2002, 36, (7), 1554-1560.

5. de Gouw, J.; Warneke, C., Measurements of volatile organic compounds in the earths atmosphere using proton-transfer-reaction mass spectrometry. *Mass Spectrometry Reviews* 2007, 26, (2), 223-257.
6. Zhu, X.; Yang, W.; Geng, C.; Han, B.; Yin, B.; Wang, X.; Wang, X.; Bai, Z., Study on the Collection Efficiency of Air Particulate Matter Sampling Filters. *Acta Scientiarum Naturalium Universitatis Nankaiensis* 2018, 51, (1), 106-111.
7. Zhang, Y. Study on speciation of particulate organic matter from combustion sources. Doctoral Dissertation, Peking University, 2006.
8. He, X.; Huang, X. H. H.; Chow, K. S.; Wang, Q.; Zhang, T.; Wu, D.; Yu, J. Z., Abundance and Sources of Phthalic Acids, Benzene-Tricarboxylic Acids, and Phenolic Acids in PM<sub>2.5</sub> at Urban and Suburban Sites in Southern China. *ACS Earth and Space Chemistry* 2018, 2, (2), 147-158.
9. Kleindienst, T. E.; Jaoui, M.; Lewandowski, M.; Offenberg, J. H.; Docherty, K. S., The formation of SOA and chemical tracer compounds from the photooxidation of naphthalene and its methyl analogs in the presence and absence of nitrogen oxides. *Atmos. Chem. Phys.* 2012, 12, (18), 8711-8726.
10. Nishino, N.; Arey, J.; Atkinson, R., Formation and Reactions of 2-Formylcinnamaldehyde in the OH Radical-Initiated Reaction of Naphthalene. *Environmental Science & Technology* 2009, 43, (5), 1349-1353.

11. Wang, L.; Arey, J.; Atkinson, R., Kinetics and Products of Photolysis and Reaction with OH Radicals of a Series of Aromatic Carbonyl Compounds. *Environmental Science & Technology* 2006, 40, (17), 5465-5471.
12. Wang, L.; Atkinson, R.; Arey, J., Dicarbonyl Products of the OH Radical-Initiated Reactions of Naphthalene and the C1- and C2-Alkylnaphthalenes. *Environmental Science & Technology* 2007, 41, (8), 2803-2810.
13. Sasaki, J.; Aschmann, S. M.; Kwok, E. S. C.; Atkinson, R.; Arey, J., Products of the Gas-Phase OH and NO<sub>3</sub> Radical-Initiated Reactions of Naphthalene. *Environmental Science & Technology* 1997, 31, (11), 3173-3179.
14. Rohrer, F.; Lu, K.; Hofzumahaus, A.; Bohn, B.; Brauers, T.; Chang, C.-C.; Fuchs, H.; Haseler, R.; Holland, F.; Hu, M.; Kita, K.; Kondo, Y.; Li, X.; Lou, S.; Oebel, A.; Shao, M.; Zeng, L.; Zhu, T.; Zhang, Y.; Wahner, A., Maximum efficiency in the hydroxyl-radical-based self-cleansing of the troposphere. *Nature Geosci* 2014, 7, (8), 559-563.
15. Lee, B. H.; Mohr, C.; Lopez-Hilfiker, F. D.; Lutz, A.; Hallquist, M.; Lee, L.; Romer, P.; Cohen, R. C.; Iyer, S.; Kurtén, T.; Hu, W.; Day, D. A.; Campuzano-Jost, P.; Jimenez, J. L.; Xu, L.; Ng, N. L.; Guo, H.; Weber, R. J.; Wild, R. J.; Brown, S. S.; Koss, A.; de Gouw, J.; Olson, K.; Goldstein, A. H.; Seco, R.; Kim, S.; McAvey, K.; Shepson, P. B.; Starn, T.; Baumann, K.; Edgerton, E. S.; Liu, J.; Shilling, J. E.; Miller, D. O.; Brune, W.; Schobesberger, S.; D'Ambro, E. L.; Thornton, J. A.,

- Highly functionalized organic nitrates in the southeast United States: Contribution to secondary organic aerosol and reactive nitrogen budgets. *Proceedings of the National Academy of Sciences* 2016, 113, (6), 1516-1521.
16. Wang, H. C.; Lu, K. D.; Chen, X. R.; Zhu, Q. D.; Chen, Q.; Guo, S.; Jiang, M. Q.; Li, X.; Shang, D. J.; Tan, Z. F.; Wu, Y. S.; Wu, Z. J.; Zou, Q.; Zheng, Y.; Zeng, L. M.; Zhu, T.; Hu, M.; Zhang, Y. H., High N<sub>2</sub>O<sub>5</sub> Concentrations Observed in Urban Beijing: Implications of a Large Nitrate Formation Pathway. *Environmental Science & Technology Letters* 2017, 4, (10), 416-420.
17. de Gouw, J. A.; Middlebrook, A. M.; Warneke, C.; Goldan, P. D.; Kuster, W. C.; Roberts, J. M.; Fehsenfeld, F. C.; Worsnop, D. R.; Canagaratna, M. R.; Pszenny, A. A. P.; Keene, W. C.; Marchewka, M.; Bertman, S. B.; Bates, T. S., Budget of organic carbon in a polluted atmosphere: Results from the New England Air Quality Study in 2002. *Journal of Geophysical Research-Atmospheres* 2005, 110, D16305, doi: 10.1029/2004jd005623.
18. Yuan, B.; Hu, W.; Shao, M.; Wang, M.; Chen, W.; Lu, S.; Zeng, L.; Hu, M., VOC emissions, evolutions and contributions to SOA formation at a receptor site in eastern China. *Atmospheric Chemistry and Physics* 2013, 13, (17), 8815-8832.
19. Seinfeld, J. H.; Pankow, J. F., Organic atmospheric particulate material. *Annual Review of Physical Chemistry* 2003, 54, 121-140.

20. O'Meara, S.; Booth, A. M.; Barley, M. H.; Topping, D.; McFiggans, G., An assessment of vapour pressure estimation methods. *Physical Chemistry Chemical Physics* 2014, 16, (36), 19453-19469.
21. Barley, M. H.; McFiggans, G., The critical assessment of vapour pressure estimation methods for use in modelling the formation of atmospheric organic aerosol. *Atmospheric Chemistry and Physics* 2010, 10, (2), 749-767.
22. Al-Naiema, I. M.; Stone, E. A., Evaluation of anthropogenic secondary organic aerosol tracers from aromatic hydrocarbons. *Atmospheric Chemistry and Physics* 2017, 17, (3), 2053-2065.
23. Zhao, Y. L.; Kreisberg, N. M.; Worton, D. R.; Isaacman, G.; Weber, R. J.; Liu, S.; Day, D. A.; Russell, L. M.; Markovic, M. Z.; VandenBoer, T. C.; Murphy, J. G.; Hering, S. V.; Goldstein, A. H., Insights into Secondary Organic Aerosol Formation Mechanisms from Measured Gas/Particle Partitioning of Specific Organic Tracer Compounds. *Environmental Science & Technology* 2013, 47, (8), 3781-3787.
24. Sander, R., Compilation of Henry's law constants (version 4.0) for water as solvent. *Atmospheric Chemistry and Physics* 2015, 15, (8), 4399-4981.
25. Liu, Y.; Wu, Z.; Wang, Y.; Xiao, Y.; Gu, F.; Zheng, J.; Tan, T.; Shang, D.; Wu, Y.; Zeng, L.; Hu, M.; Bateman, A. P.; Martin, S. T., Submicrometer Particles Are in

- the Liquid State during Heavy Haze Episodes in the Urban Atmosphere of Beijing, China. *Environmental Science & Technology Letters* 2017, 4, (10), 427-432.
26. Fountoukis, C.; Nenes, A., ISORROPIA II: a computationally efficient thermodynamic equilibrium model for  $K^+$ - $Ca^{2+}$ - $Mg^{2+}$ - $NH_4^+$ - $Na^+$ - $SO_4^{2-}$ - $NO_3^-$ - $Cl^-$ - $H_2O$  aerosols. *Atmospheric Chemistry and Physics* 2007, 7, (17), 4639-4659.
27. Liu, M.; Song, Y.; Zhou, T.; Xu, Z.; Yan, C.; Zheng, M.; Wu, Z.; Hu, M.; Wu, Y.; Zhu, T., Fine particle pH during severe haze episodes in northern China. *Geophysical Research Letters* 2017, 44, (10), 5213-5221.
28. Kautzman, K. E.; Surratt, J. D.; Chan, M. N.; Chan, A. W. H.; Hersey, S. P.; Chhabra, P. S.; Dalleska, N. F.; Wennberg, P. O.; Flagan, R. C.; Seinfeld, J. H., Chemical Composition of Gas- and Aerosol-Phase Products from the Photooxidation of Naphthalene. *The Journal of Physical Chemistry A* 2010, 114, (2), 913-934.
29. Zhang, Y. X.; Schauer, J. J.; Zhang, Y. H.; Zeng, L. M.; Wei, Y. J.; Liu, Y.; Shao, M., Characteristics of particulate carbon emissions from real-world Chinese coal combustion. *Environmental Science & Technology* 2008, 42, (14), 5068-5073.
30. Zhang, Y.-x.; Shao, M.; Zhang, Y.-h.; Zeng, L.-m.; He, L.-y.; Zhu, B.; Wei, Y.-j.; Zhu, X.-l., Source profiles of particulate organic matters emitted from cereal straw burnings. *Journal of Environmental Sciences* 2007, 19, (2), 167-175.

31. Cai, T.; Zhang, Y.; Fang, D.; Shang, J.; Zhang, Y.; Zhang, Y., Chinese vehicle emissions characteristic testing with small sample size: Results and comparison. *Atmospheric Pollution Research* 2017, 8, (1), 154-163.
32. Yang, H.; Chen, J.; Wen, J.; Tian, H.; Liu, X., Composition and sources of PM<sub>2.5</sub> around the heating periods of 2013 and 2014 in Beijing: Implications for efficient mitigation measures. *Atmospheric Environment* 2016, 124, 378-386.
33. Wang, M.; Shao, M.; Chen, W.; Yuan, B.; Lu, S.; Zhang, Q.; Zeng, L.; Wang, Q., A temporally and spatially resolved validation of emission inventories by measurements of ambient volatile organic compounds in Beijing, China. *Atmospheric Chemistry and Physics* 2014, 14, (12), 5871-5891.
34. Odum, J. R.; Hoffmann, T.; Bowman, F.; Collins, D.; Flagan, R. C.; Seinfeld, J. H., Gas/Particle Partitioning and Secondary Organic Aerosol Yields. *Environmental Science & Technology* 1996, 30, (8), 2580-2585.
35. Dzepina, K.; Volkamer, R. M.; Madronich, S.; Tulet, P.; Ulbrich, I. M.; Zhang, Q.; Cappa, C. D.; Ziemann, P. J.; Jimenez, J. L., Evaluation of recently-proposed secondary organic aerosol models for a case study in Mexico City. *Atmospheric Chemistry and Physics* 2009, 9, (15), 5681-5709.
36. Zhang, X.; Cappa, C. D.; Jathar, S. H.; McVay, R. C.; Ensberg, J. J.; Kleeman, M. J.; Seinfeld, J. H., Influence of vapor wall loss in laboratory chambers on yields of

- secondary organic aerosol. Proceedings of the National Academy of Sciences of the United States of America 2014, 111, (16), 5802-5807.
37. Zhang, J. K.; Sun, Y.; Liu, Z. R.; Ji, D. S.; Hu, B.; Liu, Q.; Wang, Y. S., Characterization of submicron aerosols during a month of serious pollution in Beijing, 2013. Atmos. Chem. Phys. 2014, 14, (6), 2887-2903.
38. Zheng, J. Source apportionment of organic aerosols and contribution of secondary formation from vehicle emissions (in Chinese). Doctoral Dissertation, Peking University, 2017.
39. Sun, Y. L.; Du, W.; Fu, P. Q.; Wang, Q. Q.; Li, J.; Ge, X. L.; Zhang, Q.; Zhu, C. M.; Ren, L. J.; Xu, W. Q.; Zhao, J.; Han, T. T.; Worsnop, D. R.; Wang, Z. F., Primary and secondary aerosols in Beijing in winter: sources, variations and processes. Atmospheric Chemistry and Physics 2016, 16, (13), 8309-8329.
40. Li, H. Y.; Duan, F. K.; He, K. B.; Ma, Y. L.; Kimoto, T.; Huang, T., Size-Dependent Characterization of Atmospheric Particles during Winter in Beijing. Atmosphere 2016, 7, (3), 11.
41. Ho, K. F.; Lee, S. C.; Ho, S. S. H.; Kawamura, K.; Tachibana, E.; Cheng, Y.; Zhu, T., Dicarboxylic acids, ketocarboxylic acids, alpha-dicarbonyls, fatty acids, and benzoic acid in urban aerosols collected during the 2006 Campaign of Air Quality Research in Beijing (CAREBeijing-2006). Journal of Geophysical Research-Atmospheres 2010, 115, D19312, doi: 10.1029/2009jd013304.

42. Ng, N. L.; Kroll, J. H.; Chan, A. W. H.; Chhabra, P. S.; Flagan, R. C.; Seinfeld, J. H., Secondary organic aerosol formation from m-xylene, toluene, and benzene. *Atmospheric Chemistry and Physics* 2007, 7, (14), 3909-3922.
43. Li, L.; Tang, P.; Nakao, S.; Cocker, D. R., III, Impact of molecular structure on secondary organic aerosol formation from aromatic hydrocarbon photooxidation under low-NO<sub>x</sub> conditions. *Atmospheric Chemistry and Physics* 2016, 16, (17), 10793-10808.
44. Chan, A. W. H.; Kautzman, K. E.; Chhabra, P. S.; Surratt, J. D.; Chan, M. N.; Crouse, J. D.; Kuerten, A.; Wennberg, P. O.; Flagan, R. C.; Seinfeld, J. H., Secondary organic aerosol formation from photooxidation of naphthalene and alkylnaphthalenes: implications for oxidation of intermediate volatility organic compounds (IVOCs). *Atmospheric Chemistry and Physics* 2009, 9, (9), 3049-3060.
45. Hu, W.; Hu, M.; Hu, W.; Jimenez, J. L.; Yuan, B.; Chen, W.; Wang, M.; Wu, Y.; Chen, C.; Wang, Z.; Peng, J.; Zeng, L.; Shao, M., Chemical composition, sources, and aging process of submicron aerosols in Beijing: Contrast between summer and winter. *Journal of Geophysical Research-Atmospheres* 2016, 121, (4), 1955-1977.
46. Sun, Y.; Wang, Z.; Dong, H.; Yang, T.; Li, J.; Pan, X.; Chen, P.; Jayne, J. T., Characterization of summer organic and inorganic aerosols in Beijing, China with an Aerosol Chemical Speciation Monitor. *Atmospheric Environment* 2012, 51, 250-259.

47. Zhang, J. K.; Ji, D. S.; Liu, Z. R.; Hu, B.; Wang, L. L.; Huang, X. J.; Wang, Y. S.,  
New characteristics of submicron aerosols and factor analysis of combined organic  
and inorganic aerosol mass spectra during winter in Beijing. *Atmos. Chem. Phys.*  
*Discuss.* 2015, 2015, 18537-18576.